ELSEVIER

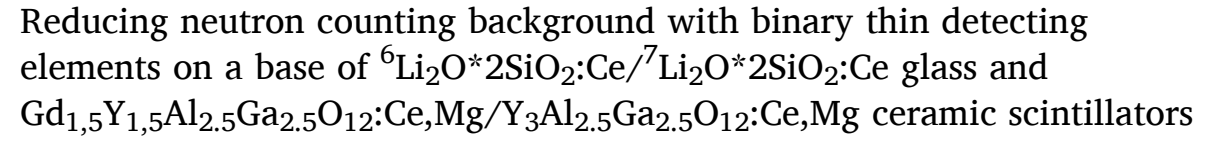
Contents lists available at ScienceDirect

# Nuclear Engineering and Technology

journal homepage: www.elsevier.com/locate/net



## Original Article





- a NRC "Kurchatov Institute", Moscow, Russia
- <sup>b</sup> Institute for Nuclear Problems, Belarus State University, Minsk, Belarus
- <sup>c</sup> ATOMTEX SPE, Minsk, Belarus
- <sup>d</sup> Mendeleev University of Chemical Technology of Russia, Moscow, Russia
- e NRC "Kurchatov Institute", B.P. Konstantinov Petersburg Nuclear Physics Institute, Gatchina, Russia
- <sup>f</sup> Physics Department, Belarus State University, Minsk, Belarus

#### ARTICLE INFO

# Keywords: <sup>6</sup>Li scintillation glass GYAGG gadolinium-Yttrium based scintillation ceramics Neutrons detection methods

#### ABSTRACT

Binary thin detecting elements on a base of  $^6\text{Li}_2\text{O}*2\text{SiO}_2:\text{Ce}/^7\text{Li}_2\text{O}*2\text{SiO}_2:\text{Ce}:\text{Ce}$  glass and  $\text{Gd}_{1.5}\text{Y}_{1.5}\text{Al}_{2.5}\text{Ga}_{2.5}\text{O}_{12}:\text{Ce}$ ,  $\text{Mg}/\text{Y}_3\text{Al}_{2.5}\text{Ga}_{2.5}\text{O}_{12}:\text{Ce},\text{Mg}$  ceramic scintillators were evaluated for detection of neutrons. Coupling in the detecting unit of neutron-sensitive and insensitive materials with separate photosensors allows the application of different techniques to discriminate gamma-rays background. Sufficient difference in scintillation kinetics of  $\text{Gd}_{1.5}\text{Y}_{1.5}\text{Al}_{2.5}\text{Ga}_{2.5}\text{O}_{12}:\text{Ce}$  and  $\text{Y}_3\text{Al}_{2.5}\text{Ga}_{2.5}\text{O}_{12}:\text{Ce},\text{Mg}$  allows pulse shape discrimination of gamma-rays of the same energy in a phoswich detecting unit when one photosensor is utilized.

#### 1. Introduction

The creation of sensitive, miniature, and inexpensive neutron counters that allow scanning the spatial distribution of their flux is of great interest. They are demanded when measuring the flux of neutrons generated by accelerator-based photoneutron sources [1–4]. Another important task is mapping the distribution of neutron fields at experimental sites of large accelerator and reactor complexes [5–8]. A progressively evolving field of measurements is the creation of neutron depth profiling instruments, especially for the inspection of lithium batteries [9–14]. Not least, we note the importance of monitoring the spatial distribution of the thermal neutron flux in the rapidly developing neutron capture therapy, where the measurement of incident, transmitted, and scattered neutron radiation is critically important [15–17]. Inorganic scintillation materials with a high concentration of nuclei of elements with a large neutron absorption cross section are promising for such measurements. There are a few such elements, but only Li and Gd

ions are suitable for creating inorganic scintillators [18]. A well-known scintillation material for neutron registration is lithium-silicate glass [19–21]. Glass, like ceramics, is a hard, chemically stable material. Another species of inorganic scintillation materials are single crystals, ceramics, and powders, which are based on activated by Ce or Tb ions compounds of the gadolinium-aluminum- gallium garnet family [22–26]. These scintillators have good sensitivity to neutrons in a wider energy range than lithium-containing materials. A common disadvantage of gadolinium-containing scintillators is their high sensitivity to background gamma radiation due to the presence of heavy gadolinium atoms in the matrix [27]. Since the secondary particles registered in the gadolinium-containing scintillator material are gamma quanta when registering neutrons up to energies of several MeV, one of the possible solutions for reducing the background in the detector is to place it in a shield made of heavy metals [28], but this makes the detector relatively buller.

The natural mixture of gadolinium isotopes contains 14.8 % of the

https://doi.org/10.1016/j.net.2025.103867

Received 29 June 2025; Received in revised form 11 August 2025; Accepted 18 August 2025 Available online 19 August 2025

1738-5733/© 2025 Korean Nuclear Society, Published by Elsevier Korea LLC. This is an open access article under the CC BY-NC-ND license (http://creativecommons.org/licenses/by-nc-nd/4.0/).



<sup>\*</sup> Corresponding author. Institute for Nuclear Problems, Belarus State University, Minsk, Belarus. *E-mail address:* vitaly.mechinsky@gmail.com (V. Mechinsky).

isotope  $^{155}$ Gd and 15.7% of the isotope  $^{157}$ Gd with thermal neutron absorption cross-sections of 61,000b and 254,000b, respectively, while they form 99.99% of the total thermal neutron absorption cross-section of the natural mixture of isotopes of  $\sim$ 49,000b.

When capture of thermal neutrons by 155Gd and 157Gd nuclei (Qvalue 8.54 and 7.94 MeV respectively) occurs, an instantaneous cascade of gamma quanta, X-rays, internal conversion (IC) electrons, and Auger electrons happens. The lower transitions that de-excite nuclei are 199 keV, 89 keV, 182 keV, and 79.5 keV [29]. In addition, the emission of the internal conversion (IC) electrons, followed by the emission of X-rays and Auger electrons occurs. In this case, with complete absorption in the detector material of the IC electrons, X-rays and Auger electrons will generate a peak in the measured spectrum with an energy equal to the sum of the simultaneously emitted X-rays and electrons [27]. According to Ref. [30], in the practically important energy range >20 keV the most probable emission is from IC electrons with energies of 29.3, 38.7, 71.9, 77.9, 81.3, 174.1 keV, X-rays with energies of 42.3, 43.0, 50.0 keV and Auger electron 34.9 keV. In the actual measured spectra, the peak from IC electrons, X-rays and Auger electrons with a total energy in the region of 80-90 keV is inseparable from the peaks from prompt gamma-emission of 79.5 keV and 89 keV. A possible solution, investigated in the present paper, is the use of closely spaced scintillation elements made of neutron-sensitive and neutron-insensitive inorganic materials, similar in composition and scintillation characteristics. Besides the thermal and epithermal neutrons, the similarity of compositions is especially important when registering fast neutrons. Fast neutrons interact with light nuclei of ligands and produce secondary charged particles, the signals of which are distinguished by the pulse shape (PSD) [31]. When combining, a neutron-sensitive detector material will detect the flux of neutrons and gamma quanta, while a neutron-insensitive one will detect only a flux of gamma quanta. At the same time, using the possible exit of secondary particles and soft photons from the volume of a neutron-sensitive material and their registration in a neutron-insensitive scintillator makes it possible to utilize time coincidences to increase the efficiency of neutron detection relative to the efficiency of gamma quanta detection.

Thus motivated, we evaluated the response of two detectors based on Hamamatsu MPPC photoreceivers. One unit consisted of two adjacent plates of  $^6\mathrm{Li}_2\mathrm{O}^*2\mathrm{SiO}_2:\mathrm{Ce}/^7\mathrm{Li}_2\mathrm{O}^*2\mathrm{SiO}_2:\mathrm{Ce}$  glass scintillators, which are entitled  $^6\mathrm{DSL}$  or  $^7\mathrm{DSL}$  (disilicate of lithium). Variation of the lithium isotope in the scintillator could make it either neutron sensitive or neutron blinded. A recently developed bright and fast scintillation ceramics  $Y_3\mathrm{Al}_{2.5}\mathrm{Ga}_{2.5}\mathrm{O}_{12}:\mathrm{Ce},\mathrm{Mg}$  (YAGG), which is insensitive to neutrons up to their energy of a few MeV, was chosen to be adjacent to  $\mathrm{Gd}_{1.5}Y_{1.5}\mathrm{Al}_{2.5}\mathrm{Ga}_{2.5}\mathrm{O}_{12}:\mathrm{Ce},\mathrm{Mg}$  (GYAGG) scintillator. The latter was produced as a ceramics scintillator as well. Conclusions made are supported by results of the measurements at certified facilities utilizing a Pu-Be neutron source.

#### 1.1. Samples

The scintillation ceramic and glass samples were prepared using the technology described in Refs. [21,32]. The amplitude spectra of the  $^{137}\text{Cs}$  source, measured with YAGG and GYAGG samples of the same thickness (1.25 mm) at room temperature by an R329 (Hamamatsu) photomultiplier (PMT) with an integration time of 7  $\mu$ s in a comparison with a CsI(Tl) scintillator with a diameter of 25.4 and a height of 25.4 mm. are shown in Fig. 1. The light yield of the reference sample was 54, 000 ph/MeV. Taking into account the spectral sensitivity of the PMT to the scintillation spectrum, the YAGG light output was evaluated to be 43,000  $\pm$  1000 ph/MeV, whereas GYAGG- 41,000  $\pm$  1000 ph/MeV. Scintillation kinetics were measured at room temperature by the method of delayed coincidences with Philips XP2020 PMT in both channels. Kinetic curves are shifted on the graph for better perception of their differences. The scintillation kinetics of YAGG is characterized by a decay constant of 40 ns, whereas the kinetics of GAGG was

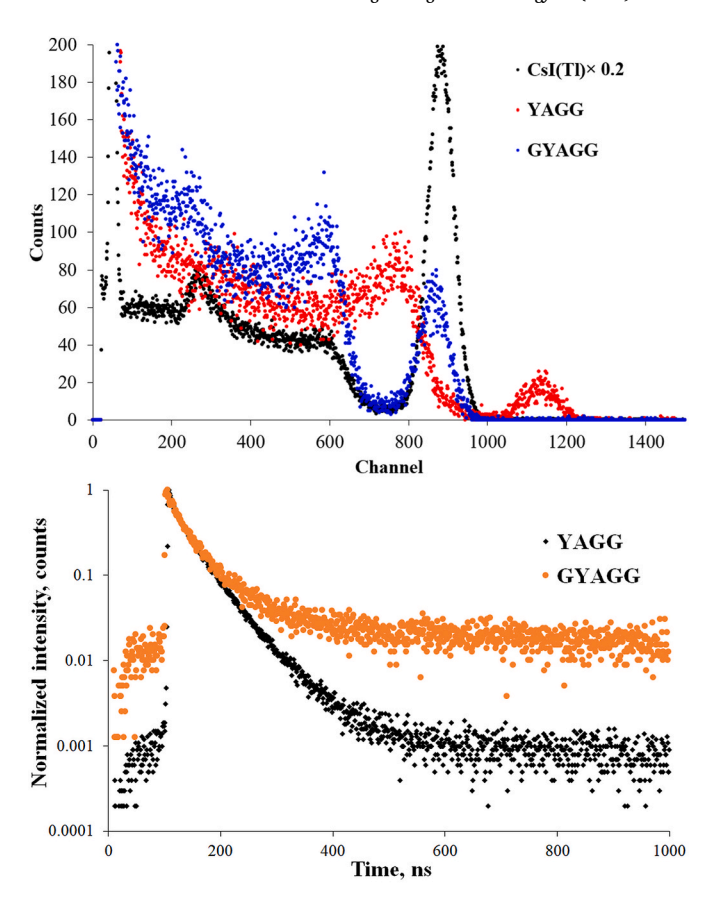


**Fig. 1.** Pulse height spectra of the 137-Cs source measured with YAGG ceramic samples in a comparison with the CsI(Tl) scintillator -a; b-scintillation kinetics of the of YAGG (triangles) and GYAGG (circles) measured at room temperature.

approximated by two exponents with  $\tau_1=38$  ns and  $\tau_2=80$  ns with fractions of 40 and 60 % correspondingly. The scintillation kinetics of YAGG are significantly shorter than the kinetics of GYAGG, which suggests the possibility of separating the signals from the two materials by the pulse shape (PSD).

To perform measurements with neutrons and gamma-quanta, a combination of a YAGG element with dimensions 1.25\*12\*12 mm with a GYAGG element of the same dimensions and 0.23 mm thick was used. The thickness of the elements was selected based on the results of modeling in the GEANT 4 package [33]. For modeling, a flat source of thermal neutrons emitted into an angle of  $2\pi$  was located at a distance of 1  $\mu$ m from the detector surface. The calculated efficiencies of thermal neutron absorption in GYAGG ceramics with a thickness of 0.05, 0.1, 0.15, 0.2, 0.5, and 1.25 mm, provided that after absorption of the neutron, gamma quanta, X-rays, and electrons left an energy of at least 15, 25, 45, 65, and 95 keV in the ceramics, are shown in Fig. 2 (a).

For GYAGG ceramics with a density of 5.86 g/cm3, the calculation of the linear attenuation coefficient based on the number of Gd atoms in 1 cm3 and a cross-section of 49,000b shows that the thermal neutron flux is attenuated by a factor of e in a layer with a thickness of  $\sim\!45~\mu m$ . For comparison, for GAGG single crystals (Gd<sub>3</sub>Al<sub>2</sub>Ga<sub>3</sub>O<sub>12</sub>:Ce) with a density of 6.68 g/cm3, such a thickness is  $\sim\!25~\mu m$ , i.e., in both cases, thermal neutrons are absorbed predominantly in the surface layer. With such thicknesses, not only high-energy gamma quanta, but also X-rays and even some energetic IC electrons have a chance to escape from the detecting element without detectable energy loss, thus reducing detecting element detection efficiency. For example,  $\sim\!40~\text{keV}$  X-rays are attenuated in e times in  $\sim\!0.33~\text{mm}$  thick Gd<sub>1.5</sub>Y<sub>1.5</sub>Al<sub>2.5</sub>Ga<sub>2.5</sub>O<sub>12</sub>:Ce,Mg.

As seen from Fig. 2(a), increasing the lower registration threshold from  $15-25\ keV-95\ keV$  reduces the registration efficiency from 26 to 28

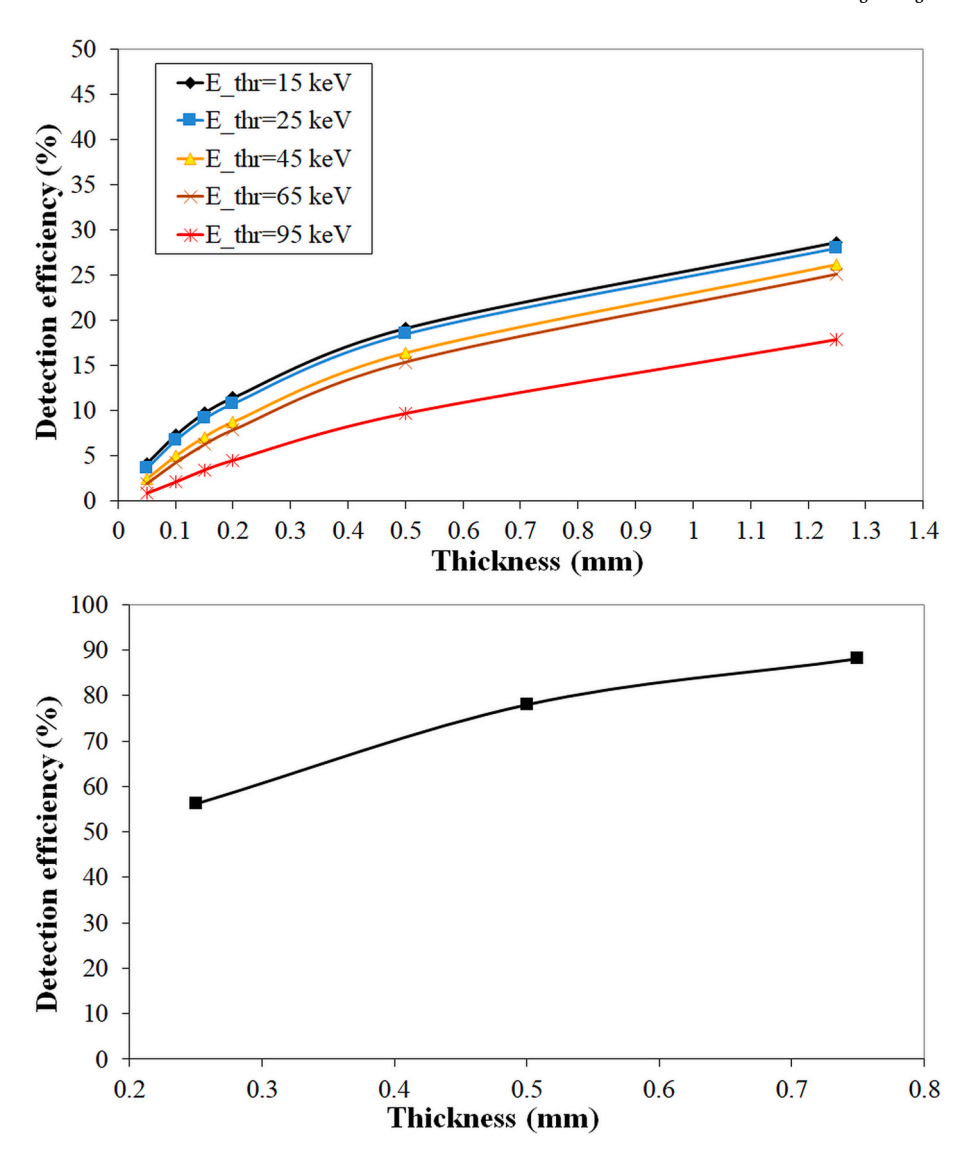


Fig. 2. GEANT4 simulated detection efficiency to thermal neutrons versus thickness: a- GYAGG ceramics plates, events are counted as detected when deposited energy in ceramics plate exceeds energy thresholds  $E_{thr} = 15, 25, 45, 65, 95 \text{ keV}$ ; b-  $^6DSL$  glass plates.

 $\%-\sim15$  % at a thickness of 1 mm. On the other hand, for a GYAGG detector element thickness of 0.1 mm, when passed neutron flux is reduced by almost 90 % at normal incidence, the detection efficiency does not exceed 8 % even at a 15 keV energy threshold. Therefore, as a compromise solution, a thickness of a thin element of 0.23 mm was chosen.

The samples of scintillation glasses  $^6\text{Li}_2\text{O}*2\text{SiO}_2$ :Ce (90 % enrichment) and  $^7\text{Li}_2\text{O}*2\text{SiO}_2$ :Ce (99.99 % enrichment) used in the pair had a size of 12\*12 mm and a thickness of 0.5 mm. The typical light yield of the lithium silica glass is 4000 ph/MeV when detecting gamma-rays and elements are characterized by non-exponential scintillation kinetics with components  $\tau 1 = 42$  ns,  $\tau 2 = 96$  ns,  $\tau 3 = 600$  ns with fractions of 48, 33, and 19 %, respectively. The thickness of the scintillation glasses was also selected based on the results of modeling in the GEANT 4 package. The results of assessing the sensitivity of 6DSL glass to thermal neutrons  $\eta(\%)$  depending on the thickness of the material are shown in Fig. 2(b). When simulating, it was assumed that after the absorption of a neutron, the reaction products left energy in the glass of at least 30 keV. It is evident that increasing the thickness by 1.5 times, from 0.5 to 0.75 mm, gives an increase in efficiency of only from 77.7 % to 87.8 %.

The measuring unit consisted of two HAMAMATSU S13361-3050AE-04 MPPC arrays, comprising 16 (4x4) MPPCs with 3  $\times$  3 mm size with

 $50~\mu m$  pixel pitch. Both arrays were connected to a 16-channel summator and to two single-channel fast preamplifiers; all summators and preamplifiers were based on AD8009 current feedback amplifiers. The preamplifier's outputs were read out with a DRS4 waveform digitizing board able to record the input signal with a sample rate between 0.7 and 5.2 GSPS. Two channels of a digitizer were used to acquire data at 1.0 GSPS in a total time scale of 1024 ns. The sketch of the detecting unit is in Fig. 3.

A neutron-sensitive detecting element was placed on one MPPC array on optical grease; an insensitive one was placed on the other. A light reflector made of 10  $\mu m$  Al foil was installed between the ceramic scintillation elements. In the case of the glass scintillators, a light reflector, Lumirror (Toray Advanced Materials Korea Inc.), 185  $\mu m$  thick, was applied. The pulse height spectra, presented in the figures below, are the spectra of the sum of 1024 digitized sample amplitudes over a 1024 ns time scale. So the pulse height spectra are "integral" height spectra, which are equivalent to charge integration over a 1024 ns time scale from the pulse beginning.

The measurements were performed at ATOMTEX certified dosimetry facilities including a  $^{238}\text{PuBe}$  based neutron dosimetry bench and  $^{137}\text{Cs}$  based gamma-dosimetry bench. At the neutron measurements detector units were placed in perpendicular to the axis of the bench:  $^{238}\text{PuBe}$ 

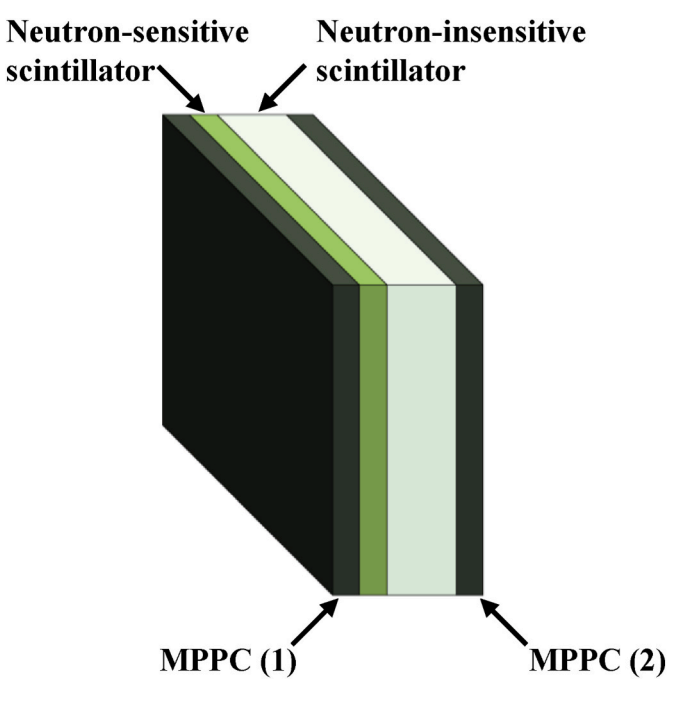


Fig. 3. Sketch of the detector assembly.

source – plastic moderator 20 cm – Cd filter 1 mm, which was used to distinguish count rates from neutrons with energies below 0.4 eV, "thermal", and above 0.4 eV, "epithermal". Neutron-sensitive detector elements were faced to the source. After plastic moderator and cadmium filter, a 5 cm lead plate coupled to the 5 mm copper sheet was mounted. This sandwich was useful to cut gamma-rays, produced in cadmium at neutron radiation capture when sensitivity was evaluated.

To evaluate a capability for PSD with neutron-sensitive and insensitive ceramic samples, an R329 PMT (Hamamatsu) coupled to DRS-4 was used. A bombardment by <sup>137</sup>Cs or <sup>241</sup>Am was applied. The GYAGG detecting element was coupled to the PMT window by optical grease, and the YAGG thin ceramics were mounted on the top surface of GYAGG with the grease between them as well. The phoswich was covered by a light reflector.

#### 2. Results and discussion

#### 2.1. Measurements with the glass-based detector assembly

Fig. 4(a) shows pulse height spectra recorded by  $a^{6,7}DSL$  scintillation glass assembly with  $a^{238}Pu$ -Be neutron source and a 20 cm polyethylene moderator. As seen, residual 6Li nuclei in  $^7DSL$  produce a little response in a comparison with the intense response of the  $^6DSL$  to neutrons peaked at 77 channels. Panel (b) in Fig. 4 rdepicts a response to a natural background of 0.1 mkSv/h measured prior to the measurements with the  $^{238}Pu$ -Be source. One can state that natural background has a very low contribution in the useful channels 40–100. Based on the natural background we have evaluated, the neutron equivalent of the 1.0 mkSv/h gamma background is  $1.12 \pm 0.08$  neutron/sm $^2 \times$  s when the total useful spectrum between #3 and #100 channels is accounted for, and  $0.19 \pm 0.04$  neutron/sm $^2 \times$  s when the neutron peak region between #40 and #100 channels is used. Both numbers turn out equal for  $^7DSL$  and  $^6DSL$  samples, and their errors are given based on the acquired statistics in Fig. 4(b) spectra.

Fig. 5 depicts the  $^6$ DSL response to  $^{238}$ Pu-Be neutrons after a 20 cm thick polyethylene moderator and with and without a 1 mm thick Cd thermal neutron filter. A spectrum of thermal neutrons with energy below 0.4 eV was obtained by extracting the spectrum recorded with a Cd filter from the spectrum recorded without a Cd filter.

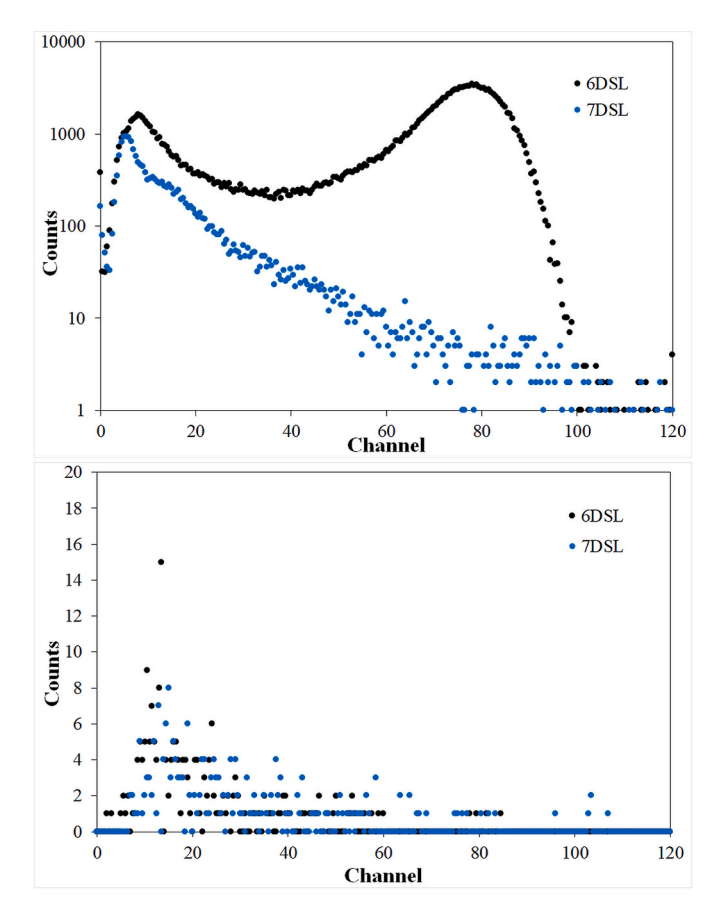


**Fig. 4.**  $^{6.7}$ DSL scintillation glasses response: a-to  $^{238}$ PuBe neutrons after 20 cm polyethylene moderator; b-to a natural background of 0.1 mkSv/h, acquisition time of 1800 s.

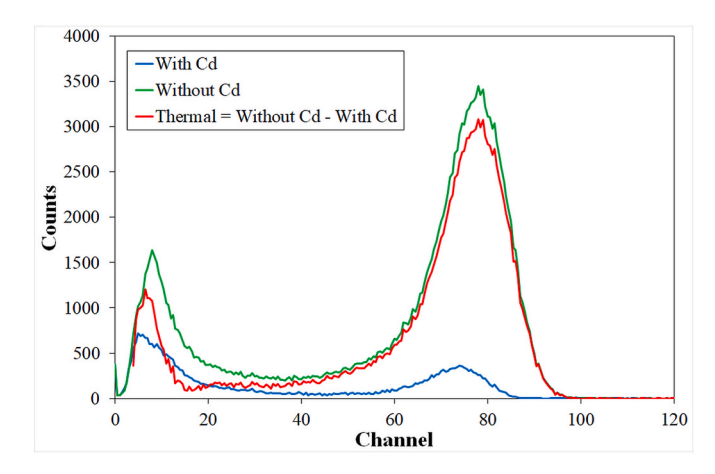


Fig. 5.  $^6$ DSL scintillator response to  $^{238}$ PuBe source neutrons after polyethylene moderator with and without 1 mm Cd filter. Acquisition time of 1800 s.

Thermal neutron flux at the measurement point was 121.6 neutrons/  $cm^2\times s$ ; this number was used to define neutron detection efficiency  $\eta$  (NDE). At the evaluation, we have taken into account the  $^6\text{DSL}$  sample area of 1.44 sm² and acquisition dead time, caused mainly by the data transfer from DRS4 and writing of the massive data file in a PC. Using the whole useful spectrum between #3 and #100 channels, NDE was evaluated to be  $\eta=69.2$ %; in other words, the sensitivity is 0.69 pulse per second for the neutron flux of 1 neutron/s  $\times$  cm², which is rather close to the simulation result presented in Fig. 3, and  $\eta=59.1$ % for the detached neutron peak between #40 and #100 channels.

As soon as <sup>7</sup>DSL and <sup>6</sup>DSL 0.5 mm glass plates have similar responses to natural gamma background according to Fig. 4(b), adding the 0.5 mm <sup>7</sup>DSL plate to the 0.5 mm <sup>6</sup>DSL plate gives a possibility to separately acquire the gamma background spectrum and extract it from the neutron + gamma spectrum acquired by the <sup>6</sup>DSL plate. The gamma suppression defined as the neutron signal (number of <sup>6</sup>DSL counts) to gamma-"noise" standard deviation (SD, root square from <sup>7</sup>DSL counts) ratio will depend on the acquired statistics. Without a <sup>7</sup>DSL channel, strictly speaking, it is impossible to attribute <sup>6</sup>DSL acquired counts either to a neutron radiation source or to high energy gamma-source.

A comparison of the  $^6$ DSL scintillation glass response to  $^{238}$ Pu-Be neutrons after a 20 cm polyethylene moderator and to  $a^{137}$ Cs gamma source is shown in Fig. 6. When the area of the neutron peak is calculated between #40 and #100 channels, the influence of  $\gamma$ -quanta from  $^{137}$ Cs on neutron counting is negligible.

#### 2.2. Measurements with the ceramics-based detector assembly

Fig. 7 shows pulse height spectra recorded with the assembly of 0.23 mm GYAGG (0.23) and 1.25 mm thick YAGG, obtained at 78.8 neutron/  $\text{sm}^2 \times \text{s}$  neutron flux, with acquisition times T = 1800 s. Channel #43 roughly corresponds to the 241Am 59.6 keV photo-absorption γ-peak. Due to some nonproportionality of the response of aluminum/gadolinium garnets in the energy range <100 keV, the precise energy scale calibration is difficult. A signal in YAGG between 50 and 80 channels is produced by escaped GYAGG secondaries. Therefore, in a such geometry, YAGG plate does not provide a possibility to separately acquire the gamma background spectrum and extract it from the neutron + gamma spectrum. Fig. 8 shows the response of the GYAGG to <sup>238</sup>PuBe neutrons after 20 cm of polyethylene moderator with and without a 1 mm Cd filter. A wide peak at around 150 channel most probably is caused by the combining of the responses to 199, 182 keV gamma-rays and IC electrons of 174.1 keV energy. These spectra were used to evaluate NDE as well.

Taking into account the GYAGG sample area of 1.44 cm $^2$  and the acquisition dead time, the neutron detection efficiency was found to be 19 %; neutron sensitivity of 0.19 pulse per second for the flux of 1 neutron/s  $\times$  cm $^2$  for the whole spectrum starting from the 15 keV energy threshold, corresponding to #11 channel in the spectrum was evaluated. According to simulations presented in Fig. 2, the expected NDE should be  $\sim$ 13 % of efficiency for the specific 0.23 mm thickness and 15 keV energy threshold. However, performed GEANT4 simulations did not take into consideration the time distribution of the emitted particles. As a result, the time coincidences of lower energy X-rays and Auger electrons with high emission rates may form useful counts above the 15 keV energy threshold.

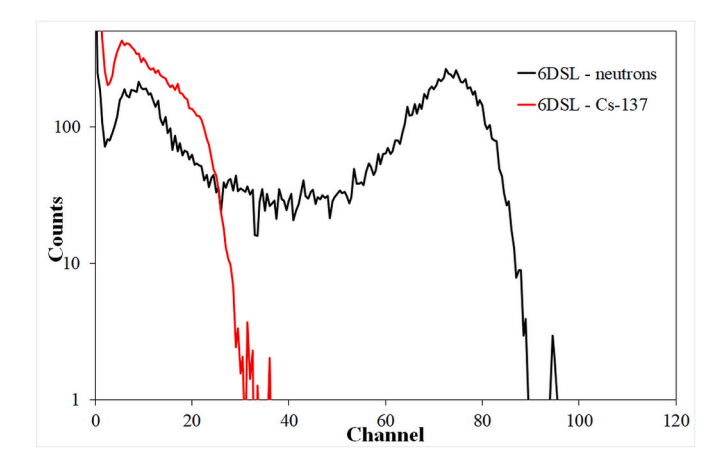
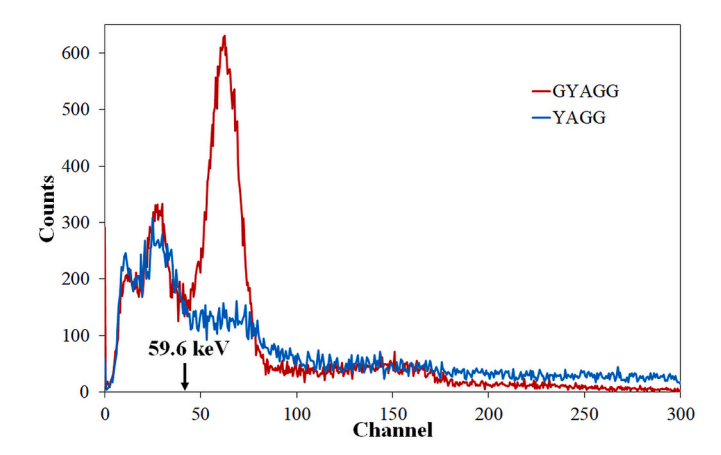


Fig. 6.  $^6 \rm DSL$  scintillation glass response to  $^{238} \rm Pu$ -Be neutrons after polyethylene moderator and to  $^{137} \rm Cs~\gamma$ -source.



**Fig. 7.** The response of the GYAGG/YAGG assembly to neutrons of the  $^{238}$ Pu-Be source at a point with a 78.8 neutron/sm<sup>2</sup>  $\times$  s flux with an acquisition time of 1800 s.

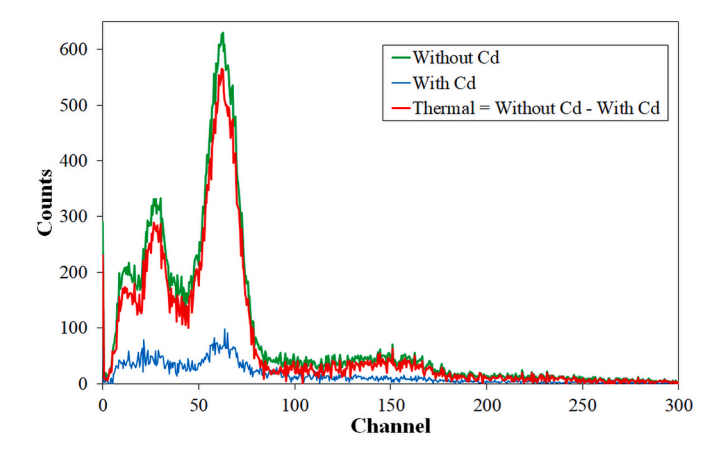


Fig. 8. The GYAGG response to  $^{238}$ PuBe source neutrons after 20 cm of polyethylene moderator with and without a 1 mm Cd filter.

Fig. 9 exhibits pulse height spectra recorded with the assembly and processed in coincidence mode with the coincidence time gate 1024 ns. A calculated neutron detection efficiency of 0.23 mm GYAGG was found to be  $\eta=4.1$ % for the whole spectrum starting from a 15 keV energy threshold and  $\eta=5.2$ % for the 1.25 mm YAGG detecting element. Therefore, in the used geometry, a sensitivity in coincidence mode is

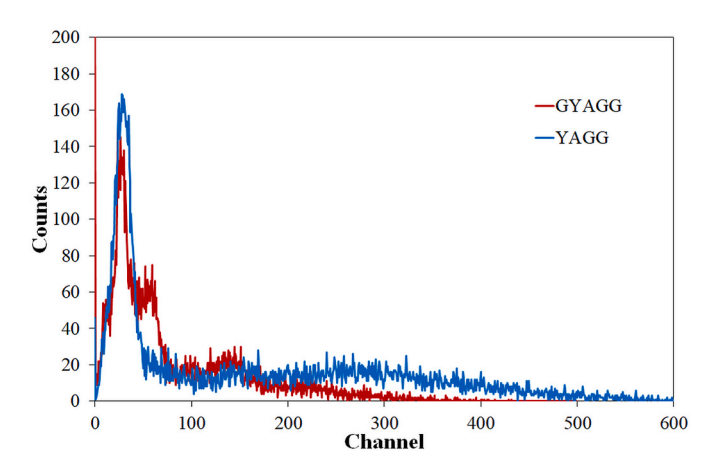


Fig. 9. Pulse height spectra recorded with the assembly GYAGG/YAGG ceramic scintillators and processed in coincidence mode. Neutron flux 78.8 neutron/  $sm^2\times s$ , acquisition times  $T=1800\,s$ , coincidence time gate  $\Delta T_{coinc.}=1024\,ns$ .

0.041 and 0.052 pulse per second for the neutron flux of 1 neutron/s  $\times$  cm² for GYAGG and YAGG correspondingly. An excess of the  $\eta$  in YAGG to GYAGG is explained by a larger volume of the neutron insensitive plate and, consequently, a high probability to detect secondaries escaping the neutron sensitive plate.

Fig. 10 illustrates the amplitude spectra of  $a^{137}$ Cs  $\gamma$ -source providing a dose rate of 3.1 mkSv/h in the position of the assembly of ceramic scintillator elements; panel 10(b) shows the coincidence- and 10(c) anticoincidence-processed spectra.

Following data presented in Fig. 10 (a) the calculated count rates from  $^{137}$ Cs gamma-source with dose rate 1.0 mkSv/h are:  $0.26 \text{ s}^{-1}\text{cm}^{-2}$  for 0.23 mm GYAGG detecting element, and 1.01 s $^{-1}\text{cm}^{-2}$  for 1.25 mm  $Y_3\text{Al}_{2.5}\text{Ga}_{2.5}\text{O}_{12}$ :Ce,Mg ceramics.

While the coincidence mode of the data processing was applied, the calculated count rates from  $^{137}\text{Cs}$  gamma-source with dose rate 1.0 mkSv/h are:  $0.075~\text{s}^{-1}\text{cm}^{-2}$  for 0.23~mm Gd\_1.5Y1.5Al\_2.5Ga2.5O12:Ce,Mg, and  $0.102~\text{s}^{-1}\text{cm}^{-2}$  for 1.25~mm Y\_3Al\_2.5Ga2.5O12:Ce,Mg ceramics. These count rates are 3.5 times for Gd\_1.5Y1.5Al\_2.5Ga2.5O12:Ce,Mg and 10 times smaller for Y\_3Al\_2.5Ga2.5O12:Ce,Mg without time selection. As a result, at the neutron counting from YAGG layer in coincidence mode, we reduce sensitivity by 3.65 times, 19 %/5.2 % = 3.65, but simultaneously reduce sensitivity to  $^{137}\text{Cs}$  gammas in this layer by factor of ten. Signal-to-noise ratio becomes slightly worse. This situation can be improved by further thickening of YAGG layer.

Another possibility to reduce sensitivity to gamma-rays is a simultaneous measurement of gamma-background by recording the pure gamma signal from YAGG layer data in anti-coincidence mode, Fig. 10 (c). When the neutron signal is recorded from the YAGG layer in the coincidence mode, and gamma-background signal is taken from YAGG layer in anti-coincidence mode, then the ratio of gamma-backgrounds in Fig. 10(b) (red) and Fig. 10(c) (blue) is found to be 1:12. This ratio in taken into account; therefore, the corrected neutron equivalent of 1.0 mkSv/h gamma background is estimated to be  $0.075/12^{\circ.5} = 0.022$  neutron/sm<sup>2</sup> × s.

Ceramic detector elements were also tested in the form of a phoswich using a single photodetector. The spectra were analyzed using the technique described in Ref. [31]. Fig. 11 shows 2-D histograms measured with  $^{137}\text{Cs}$  and  $^{241}\text{Am}$  sources, as well as histogram slices 100 ns after the start of recording.

The energy of 59.6 keV of the <sup>241</sup>Am source is close enough to the energy of the main peak produced by the secondaries in scintillation neutron-sensitive ceramics; it is obvious that these events can be distinguished in GYAGG and YAGG. Even better, are distinguished both Compton events and photoabsorption events with increasing gammaquantum energy, as seen from the data obtained under 662 keV gamma-rays.

#### 3. Conclusions

The response of detecting units consisting of paired thin detecting elements on a base of  $^6\mathrm{Li}_2\mathrm{O}*2\mathrm{SiO}_2$ :Ce/ $^7\mathrm{Li}_2\mathrm{O}*2\mathrm{SiO}_2$ :Ce or  $\mathrm{Gd}_{1.5}\mathrm{Y}_{1.5}\mathrm{Al}_{2.5}\mathrm{Ga}_{2.5}\mathrm{O}_{12}$ :Ce,Mg/Y $_3\mathrm{Al}_{2.5}\mathrm{Ga}_{2.5}\mathrm{O}_{12}$ :Ce,Mg inorganic scintillators to neutrons was evaluated. It was found that glass-detecting elements have similar responses to natural gamma background; therefore, utilizing the neutron-insensitive detecting element on a base of  $^7\mathrm{Li}$  isotope gives a possibility to separately acquire the gamma-rays background spectrum and extract it from the neutron + gamma-rays background spectrum acquired by the  $^6\mathrm{Li}$ -based detecting plate. Apparently, granularity of the detector can be regulated to meet the requirements of the neutron flux monitoring process.

In a case of the ceramic detecting elements application, it was shown that in the geometry of the closely mounted plates, the YAGG plate does not provide a possibility to separately acquire the gamma-ray background spectrum because of the signals of the secondaries escaping from the neutron-sensitive plate. However, it gives an opportunity to use coincidence and anticoincidence modes in the analysis of the pulses. This finding allowed reducing the neutron equivalent of 1.0 mkSv/h gamma-rays background to the level of 0.022 neutron/sm $^2 \times$  s when a

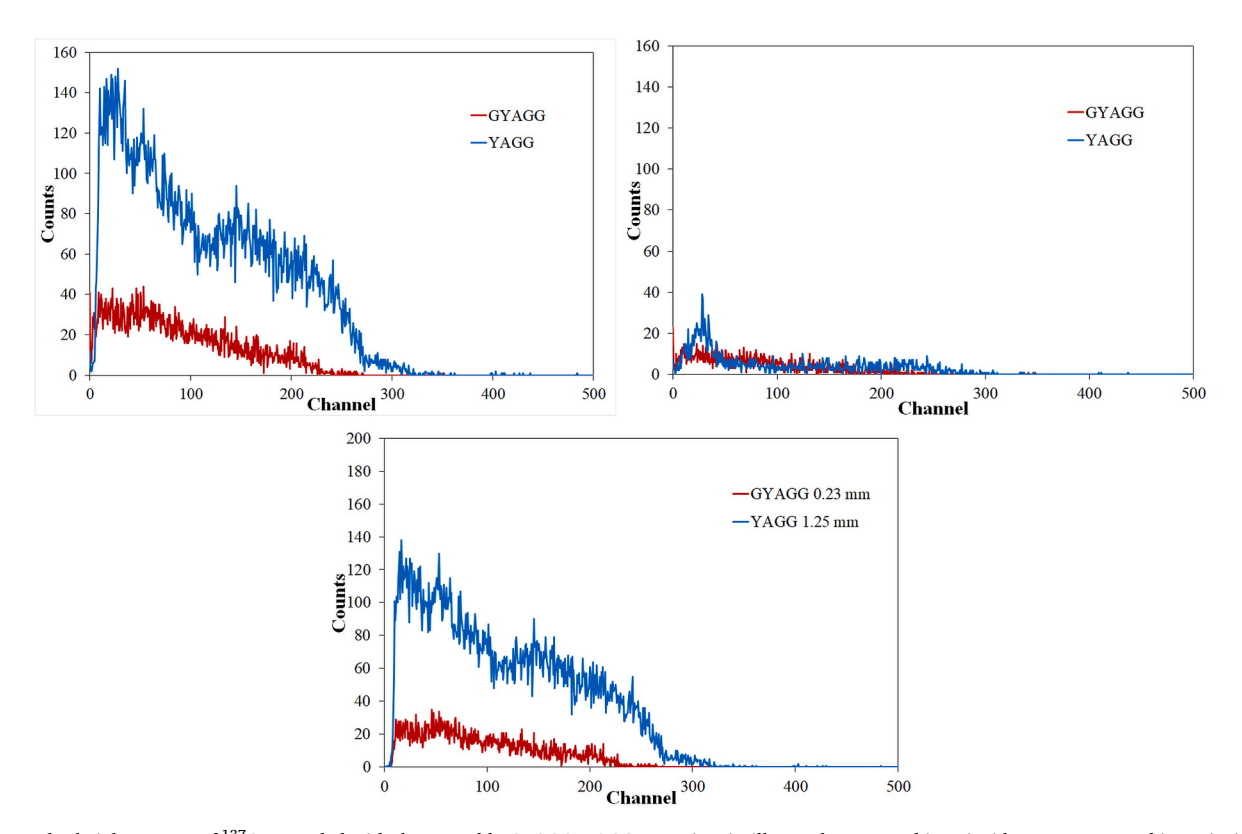


**Fig. 10.** a- Pulse height spectra of <sup>137</sup>Cs recorded with the assembly GYAGG/YAGG ceramic scintillators, b-processed in coincidence, c-processed in anticoincidence mode at coincidence time gate 1024 ns, acquisition time is 1800 s.

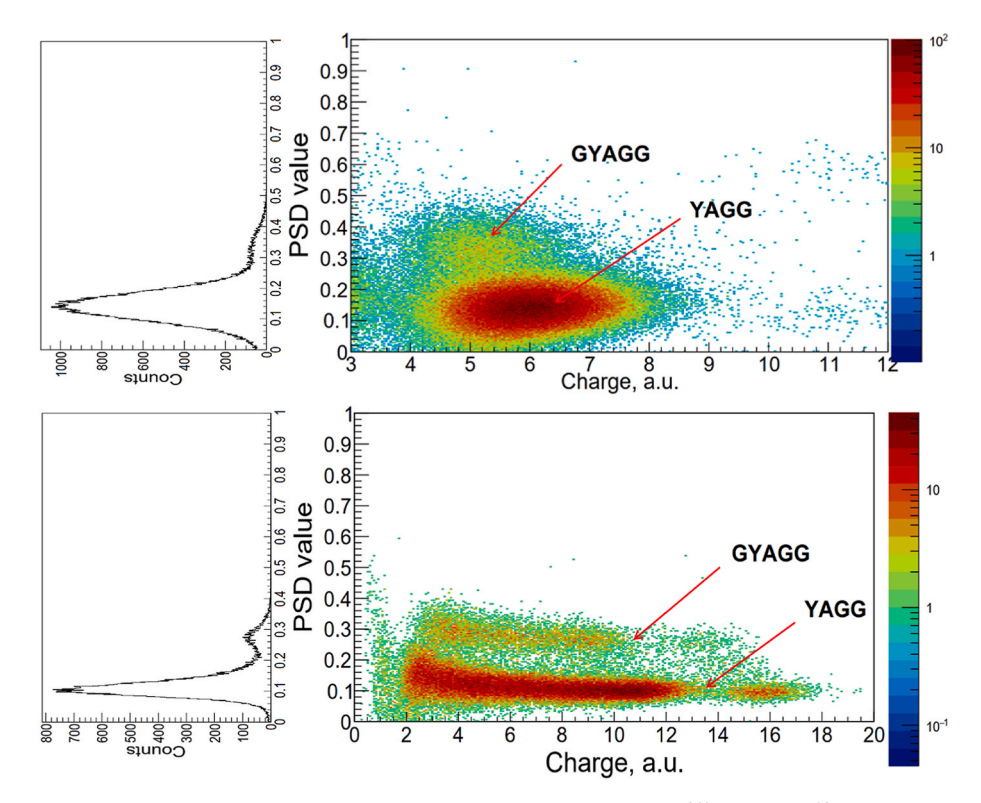


Fig. 11. 2-D histograms PSD value versus integral (right) and figures of merit (left) measured with <sup>241</sup>Am (a) and <sup>137</sup>Cs (b) with GYAGG/YAGG phoswich.

 $0.23\,$  mm plate of GYAGG was used to detect neutrons. Further improvement of the parameter may be obtained by involving in the analysis discrimination of the pulses by shape. A distinction of gammaray signals having low (59.6 keV) or high (662 keV) energy in each plate of coupled in phoswich ceramic scintillators has been demonstrated when one photoreceiver was used.

#### CRediT authorship contribution statement

Vitaly Mechinsky: Investigation. Elizaveta Borisevich: Software, Investigation. Andrei Fedorov: Writing – original draft, Methodology, Formal analysis. Olga Akimova: Investigation. Dmitry Gorshkov: Investigation. Ilya Lagutskiy: Investigation. Petr Karpyuk: Investigation. Damian Komar: Investigation. Valery Kozemiakin: Supervision. Ilya Komendo: Investigation. Ksenia Okhotnikova: Software, Investigation, Formal analysis. Vasilii Retivov: Investigation. Valentina Smyslova: Investigation. Andrey Timoshchenko: Validation, Supervision. Mikhail Korzhik: Writing – review & editing, Supervision, Methodology.

### Declaration of competing interest

The authors declare that they have no known competing financial interests or personal relationships that could have appeared to influence the work reported in this paper.

#### Acknowledgements

The research was supported by the Russian Science Foundation, grant  $N^{\circ}$  25-73-30014 https://rscf.ru/en/project/25-73-30014/

#### References

[1] V.L. Chakhlov, Z.W. Bell, V.M. Golovkov, M.M. Shtein, Photoneutron source based on a compact 10MeV, Nucl. Instrum. Methods Phys. Res. Sect. A Accel. Spectrom. Detect. Assoc. Equip. 422 (1–3) (1999) 5–9, https://doi.org/10.1016/S0168-9002 (98)01106-1.

- [2] M. Tatari, A.H. Ranjbar, Design of a photoneutron source based on 10MeV electrons of radiotherapy linac, Ann. Nucl. Energy 63 (2014) 69–74, https://doi. org/10.1016/j.anucene.2013.07.025.
- [3] Yigang Yang, Yuanjing Li, Haidong Wang, Tiezhu Li, Bin Wu, Explosives detection using photoneutrons produced by X-rays, Nucl. Instrum. Methods Phys. Res. Sect. A Accel. Spectrom. Detect. Assoc. Equip. 579 (1) (2007) 400–403, https://doi.org/ 10.1016/j.nima.2007.04.087.
- [4] S. Kutsaev, R. Agustsson, A. Arodzero, S. Boucher, J. Hartzell, A. Murokh, F. O'Shea, A.Yu Smirnov, Electron accelerators for novel cargo inspection methods, Phys. Procedia, 90,2017, 115-125,https://doi.org/10.1016/j.phpro.2017.09.036.
- [5] https://www.pnpi.nrcki.ru/en/facilities/reactor-pik visited 22.5.25.
- [6] http://english.ihep.cas.cn/csns/fa/ts/ visited 22.5.25.
- [7] https://neutrons.ornl.gov/sns visited 22.5.25.
- [8] https://ess.eu/science-instruments visited 22.5.25.
- [9] https://scintacor.com/applications/x-ray-and-neutron-screens-for-lithium-ion-battery-inspection/visited 22.5.25.
- [10] H. Nozaki, H. Kondo, T. Shinohara, et al., In situ neutron imaging of lithium-ion batteries during heating to thermal runaway, Sci. Rep. 13 (2023) 22082, https://doi.org/10.1038/s41598-023-49399-1.
- [11] M. Trunk, M. Wetjen, L. Werner, R. Gernhäuser, B. Märkisch, Zs Revay, H. Gasteiger, R. Gilles, Materials science applications of neutron depth profiling at the PGAA facility of Heinz maier-leibnitz zentrum, Mater. Char. 146 (2018) 127–134. https://doi.org/10.1016/j.matchar.2018.09.030.
- [12] L. Werner, M. Trunk, R. Gernhäuser, R. Gilles, B. Märkisch, Zs Revay, The new Neutron depth profiling instrument N4DP at the Heinz maier-leibnitz zentrum, Nucl. Instrum. Methods A 911 (2018) 30–36, https://doi.org/10.1016/j. nima 2018 09 113
- [13] R. Neagu, S. Golenev, L. Werner, C. Berner, R. Gilles, Z. Revay, L. Ziegele, J. Plomp, B. Märkisch, R. Gernhäuser, 4D tomography for neutron depth profiling applications, Nucl. Instrum. Methods Phys. Res. Sect. A Accel. Spectrom. Detect. Assoc. Equip. 1065 (2024) 169543, https://doi.org/10.1016/j.nima.2024.169543.
- [14] Jason Siegel, Xinfan Lin, Anna Stefanopoulou, Daniel Hussey, David Jacobson, David Gorsich, Neutron imaging of lithium concentration in LFP pouch cell battery, J. Electrochem. Soc. 158 (2011) A523–A529, https://doi.org/10.1149/1.3566341.
- [15] David J. Brenner, Eric J. Hall, Secondary neutrons in clinical proton radiotherapy: a charged issue, Radiother. Oncol. 86 (2) (2008) 165–170, https://doi.org/ 10.1016/j.radonc.2007.12.003.
- [16] Jason K. Rockhill, George E. Laramore, Chapter 20 neutron radiotherapy, in: Editor(s), Leonard L. Gunderson, Joel E. Tepper (Eds.), Clinical Radiation Oncology, fourth ed., Elsevier, 2016, pp. 373–380.e2, https://doi.org/10.1016/ B978-0-323-24098-7.00020-4.
- [17] Rolf F. Barth, Boron neutron capture therapy at the crossroads: challenges and opportunities, Appl. Radiat. Isot., Volume 67, Issues 7–8, Supplement, 2009, S3-S6, https://doi.org/10.1016/j.apradiso.2009.03.102.
- [18] P. Lecoq, A. Gektin, M. Korzhik, Inorganic Scintillators for Detector Systems; Particle Acceleration and Detection, Springer International Publishing, Cham, 2017, ISBN 978-3-319-45521-1.

- [19] A.R. Spowart, Neutron scintillating glasses: part 1: activation by external charged particles and thermal neutrons, Nucl. Instrum. Methods 135 (3) (1976) 441–453, https://doi.org/10.1016/0029-554X(76)90057-4.
- [20] A.R. Spowart, Neutron scintillating glasses: part III. Pulse decay time measurements at room temperature, Nucl. Instrum. Methods Phys. Res. 150 (1978) 159–163.
- [21] Y. Tratsiak, A. Fedorov, G. Dosovitsky, O. Akimova, E. Gordienko, M. Korjik, V. Mechinsky, E. Trusova, Scintillation efficiency of binary Li2O-2SiO2 glass doped with Ce3+ and Tb3+ ions, J. Alloys Compd. 735 (2018) 2219–2224, https://doi. org/10.1016/j.jallcom.2017.11.386.
- [22] M. Korjik, et al., Detection of neutrons in a wide energy range with crystalline Gd<sub>3</sub>Al<sub>2</sub>Ga<sub>3</sub>O<sub>12</sub>, Lu<sub>2</sub>SiO<sub>5</sub> and LaBr<sub>3</sub> doped with Ce scintillators, Nucl. Instr. and Meth. Phys. Res.A 931 (2019) 88–91, https://doi.org/10.1016/j. nima.2019.04.034.
- [23] Korjik, et al., Compact and effective detector of the fast neutrons on a base of Cedoped Gd<sub>3</sub>Al<sub>2</sub>Ga<sub>3</sub>O<sub>12</sub> scintillation crystal, IEEE Trans. Nucl. Sci. 66 (1) (2019) 536–540, https://doi.org/10.1109/TNS.2018.2888495.
- [24] R.S. Woolf, B.F. Phlips, A.L. Hutcheson, L.J. Mitchell, E.A. Wulf, High-Energy Neutron Response of the HR-GAGG Scintillation Crystal, IEEE Nuclear Science Symposium and Medical Imaging Conference (NSS/MIC), Boston, MA, USA, 2020, pp. 1–3, https://doi.org/10.1109/NSS/MIC42677.2020.9507839, 2020.
- [25] C.L. Wang, "Can Ce:Gd<sub>3</sub>Al<sub>2</sub>Ga<sub>3</sub>O<sub>12</sub> scintillators detect thermal neutrons?. 2019 IEEE Nuclear Science Symposium and Medical Imaging Conference NSS/MIC), Manchester, UK, 2019, pp. 1–4, https://doi.org/10.1109/NSS/ MIC42101.2019.9059730.
- [26] M. Korzhik, P. Karpyuk, A. Bondarau, A. Ilyushin, I. Kamenskikh, D. Lelekova, V. Pustovarov, V. Retivov, V. Smyslova, D. Tavrunov, A. Vasil'ev, Crosssensitization of Ce3+ and Tb3+ luminescence in (Gd, Y)3Al2Ga3O12 scintillation

- ceramics, J. Lumin. 265 (2024) 120226, https://doi.org/10.1016/j.ilumin.2023.120226.
- [27] A. Fedorov, V. Gurinovich, V. Guzov, G. Dosovitskiy, M. Korzhik, V. Kozhemyakin, A. Lopatik, D. Kozlov, V. Mechinsky, V. Retivov, Sensitivity of GAGG based scintillation neutron detector with SiPM readout, Nucl. Eng. Technol. 52 (10) (October 2020) 2306–2312.
- [28] A Method of the Registration of Neutrons and a Device for its Implementation, RU 2663683 C1.
- [29] J. Dumazert, R. Coulon, Q. Lecomte, G.H.V. Bertrand, M. Hamel, Gadolinium for neutron detection in current nuclear instrumentation research: a review, Nucl. Instrum. Methods Phys. Res. A 882 (2018) 53–68.
- [30] J. Dumazert, R. Coulon, Q. Lecomte, G.H.V. Bertrand, M. Hamel, Gadolinium for neutron detection in current nuclear instrumentation research: a review, Nucl. Instrum. Methods Phys. Res. A 882 (2018) 53–68.
- [31] A. Fedorov, A. Bondarau, A. Dzhurik, V. Bogomolov, A. Iyudin, Yu Kashchuk, V. Mechinsky, S. Obudovsky, S. Svertilov, Y. Wu, D. Yanushevich, M. Korzhik, Pulse shape discrimination at the registration of 14.6 MeV neutrons with Gd3Al2Ga3O12:Ce/SiPM(PMT) detectors, Nucl. Instrum. Methods Phys. Res. Sect. A Accel. Spectrom. Detect. Assoc. Equip. 1062 (2024) 169155, https://doi.org/10.1016/j.nima.2024.169155.
- [32] M. Korzhik, V. Retivov, V. Dubov, V. Ivanov, I. Komendo, D. Lelekova, P. Karpyuk, V. Mechinsky, A. Postupaeva, V. Smyslova, V. Shlegel, I. Spinkov, A. Vasil'ev, Compositional disordering: nanoscale engineering of advanced crystalline scintillation materials, J. Appl. Phys. 137 (2) (2025) 020701, https://doi.org/10.1063/5.0238695
- [33] S. Agostinelli, et al., GEANT4 a simulation toolkit, Nucl. Instrum. Methods Phys. Res. Sect. A Accel. Spectrom. Detect. Assoc. Equip. 506 (2003) 250–303, https://doi.org/10.1016/S0168-9002(03)01368-8.